Supplementary information

Exploiting anion and cation redox chemistry in lithium-rich perovskite oxalate: A novel next-generation Li/Na-ion battery electrode

Atin Pramanik,[a] Alexis G. Manche,[a,b] Rebecca Clulow,[a,c] Philip Lightfoot,[a] and Anthony Robert Armstrong[a,b]**

[a]School of Chemistry, University of St Andrews, St Andrews, Fife KY16 9ST, United Kingdom

[b] The Faraday Institution, Quad One, Harwell Science and Innovation Campus, Didcot, OX11 0RA, United Kingdom

[c]Department of Chemistry – Ångström Laboratory, Uppsala University, Box 538, 751 21, Uppsala, Sweden

* pl@st-andrews.ac.uk (PL), ara@st-andrews.ac.uk (ARA)

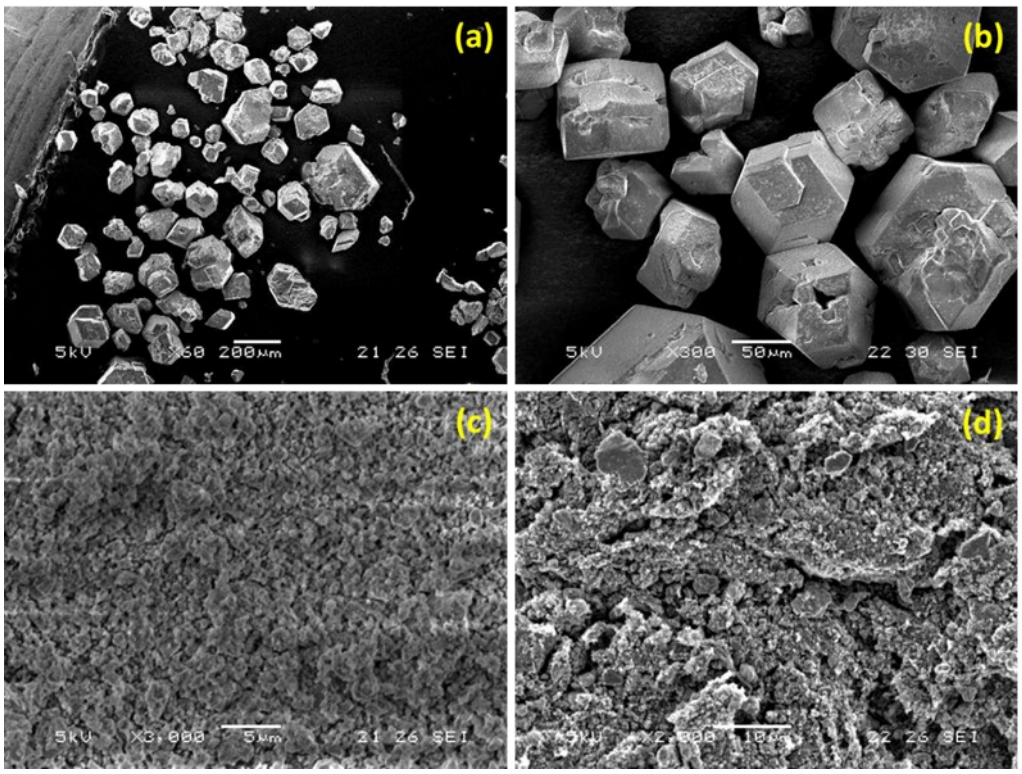

Fig. S1 SEM images of $KLi_3Fe(C_2O_4)_3$, (a) and (b) as-synthesized KLFC pristine compound at low and high magnification, (c) after ball-milling, and (d) composite with conductive Super C65 carbon black.

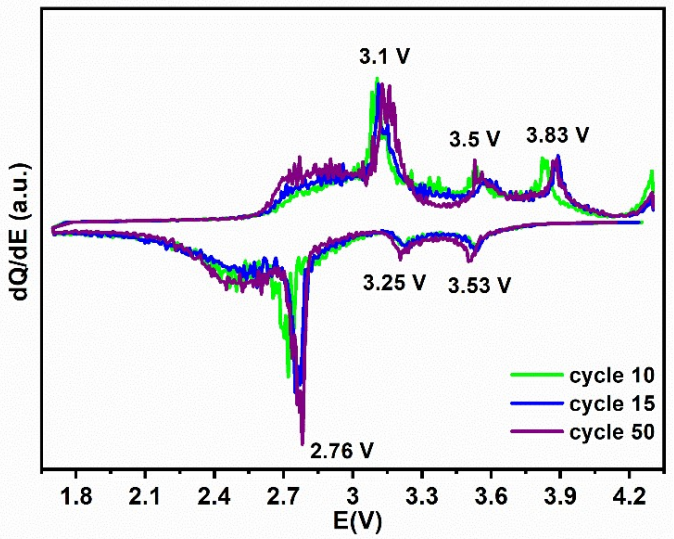

Fig. S2 Differential capacity plots of 10th, 15th, 50th cycles at 1.7-4.3 V potential window and 10 mA g^{-1} current rate for NIB.

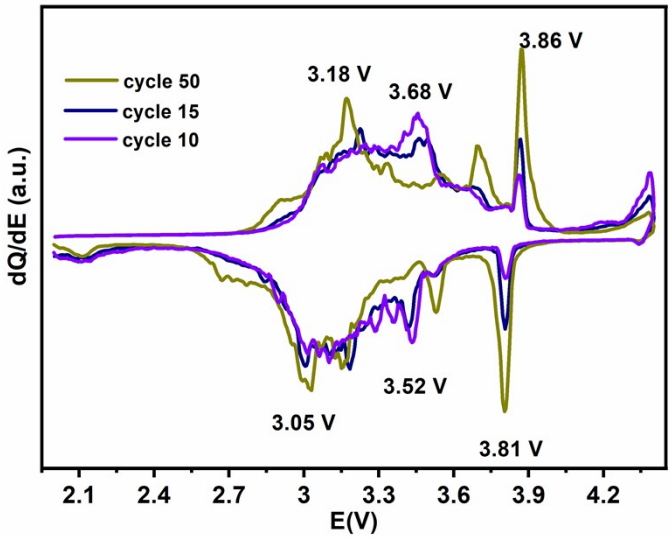

Fig. S3 Differential capacity plots of 10th, 15th, 50th cycles at 2.0-4.4 V potential window at 10 mA g^{-1} current rate for LIB.

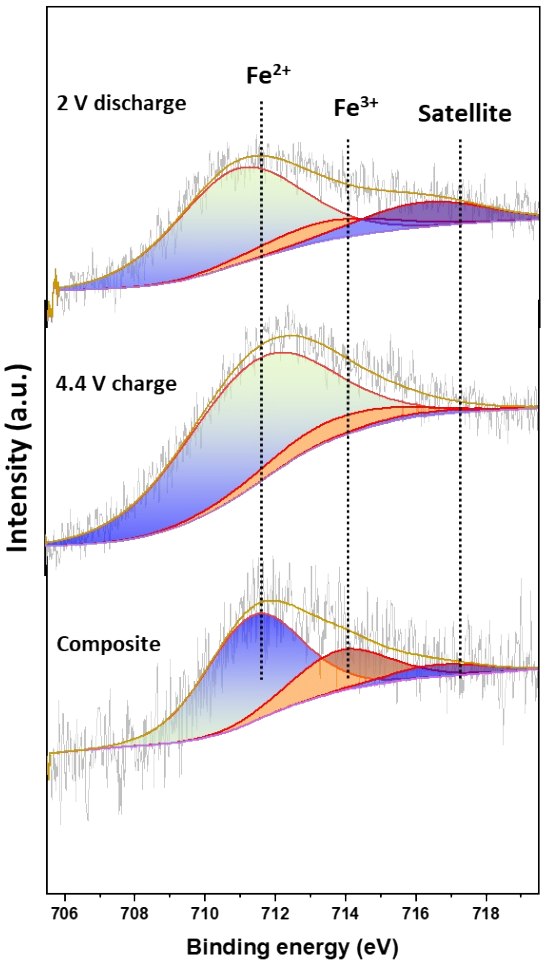

Fig. S4 Electrochemical LIB storage mechanism by XPS analysis of KLFC electrode. XPS spectra of Fe 2*p* and corresponding ratios of Fe^{2+} and Fe^{3+} for composite, charge and discharge samples.

The charge storage mechanism was characterised via ex-situ XPS analysis for LIB (Figure S2). The composite sample reveals domination of Fe^{2+} (binding energy 710.6 eV) with a lower amount of Fe^{3+} (binding energy 713.2 eV), which could be due to the surface oxidation of KLFC sample. The 10^{th} cycle fully charged state sample shows strengthening of the peak at 713.3 eV binding energy, which suggests incomplete oxidation. Similarly, the fully discharged state sample reveals a strong peak at 710.5 eV which confirms the reduction of Fe^{3+} to Fe^{2+}, and concurrent decrease of Fe^{3+}. The partial oxidation/reduction process does not satisfy the capacity obtained, which may suggest the presence of anion redox (oxalate redox).

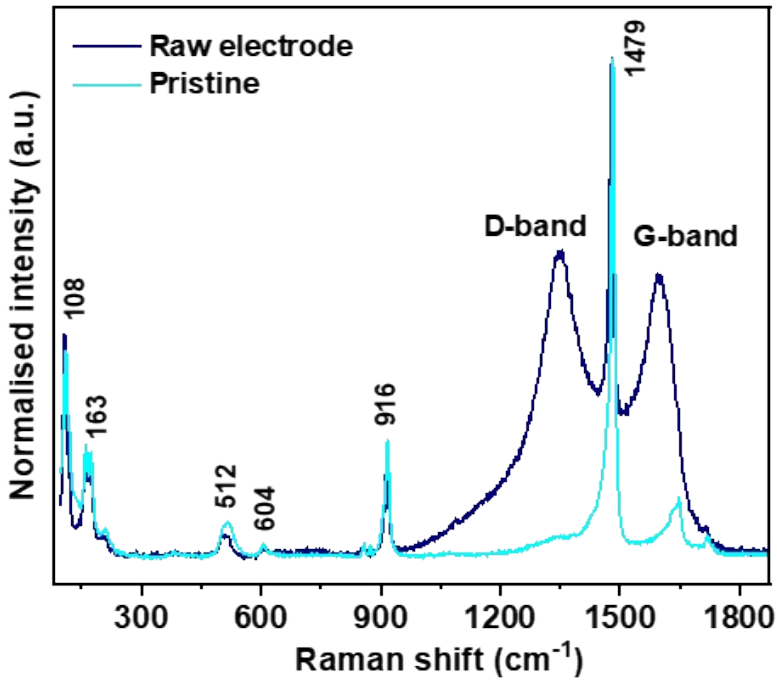

Fig. S5 Raman spectra of the pristine and raw electrodes.

Fig. S6 Raman spectrum of pure KLFC crystallites from 200 −1850 cm^{-1}.

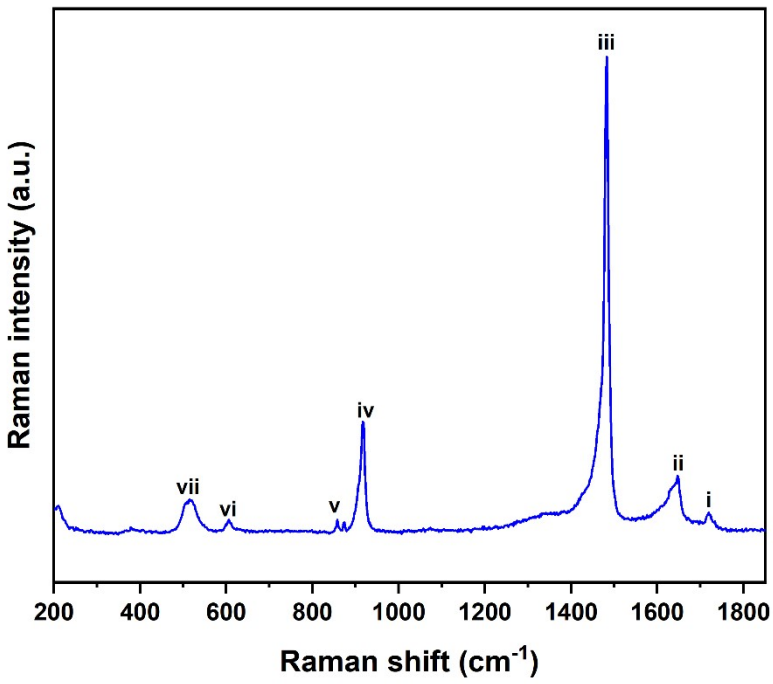

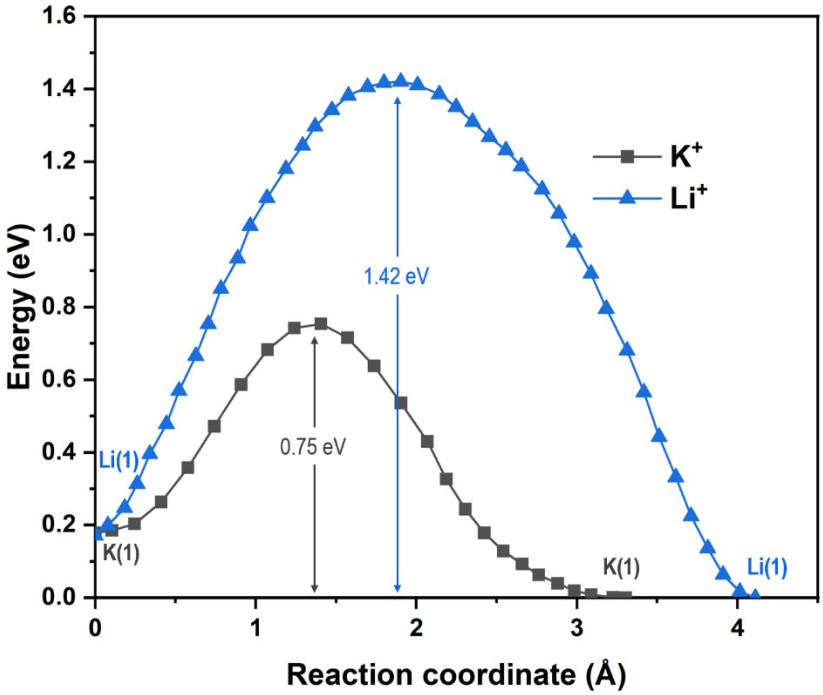

Fig. S7 Migration barriers along the Li^+ and K^+ ions pathways in KLFC as calculated by Bond-valence pathway analyzer using SoftBV software.[7-9]

K^+ and Li^+ ion migration energies are calculated by the bond valence site energy (BVSE) method as implemented in the SoftBV-GUI software. The principle of the BVSE method is to calculate the BVSE from individual bond valence sums (BVS) across plausible migration pathways. This tool is particularly useful to confirm that the K^+ ions are the most favourable to be mobile during electrochemical cycling as they have a lower energy barrier value compared to that of Li^+ ions (0.75eV for K^+ *vs.* 1.42eV for Li^+).

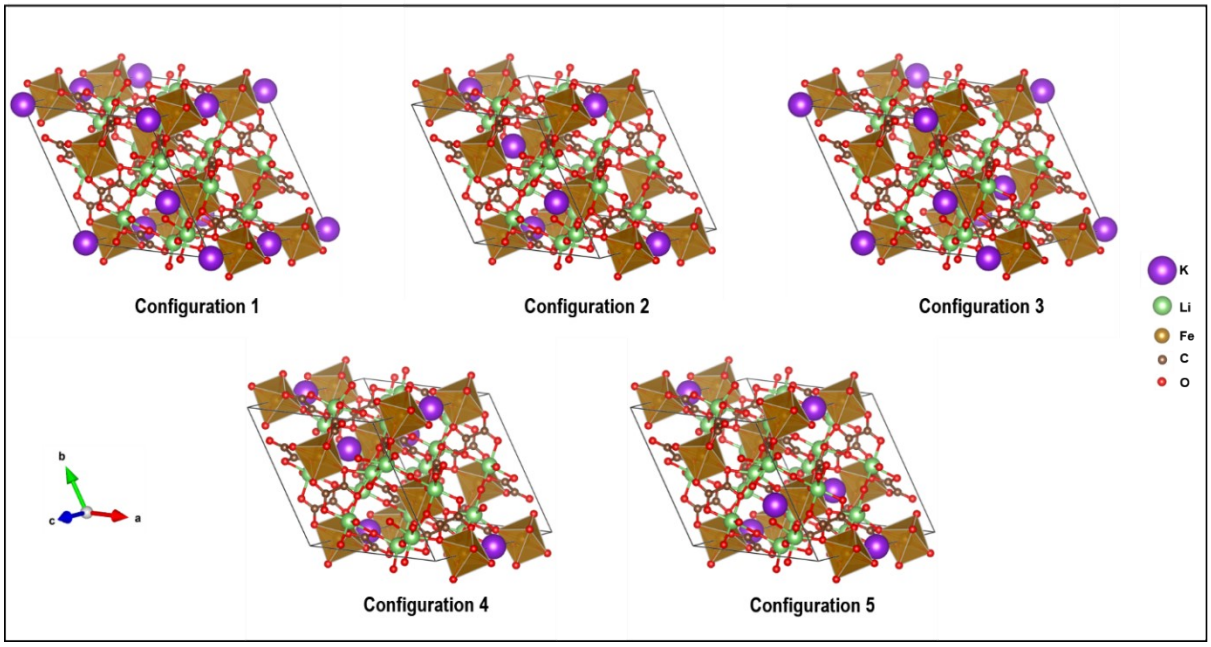

Fig. S8 Five different structure configurations of K^+ ions at 50% occupation and vacancies of KLFC.

The particularly stable framework of the KLFC structure between the initial and final states means that there is no major difference between the different possible configurations of the intermediate states. Thus, there are no major changes in lattice parameters or even in energy between the different possible configurations at the same level of occupation of K^+ ions and vacancies (see Table S1). It can thus be estimated from these examples that all the configurations would be possible experimentally and therefore to facilitate the cost of calculations, no precise configuration has been favoured for the different occupations of K^+ ions.

Table S1. Lattice parameters and energy values of different configurations of K^+ ions within the KLFC structure at 50% occupation of K^+ ions and vacancies.

Configuration	**1 (used for calculations)**	**2**	**3**	**4**	**5**
***a*(Å)**	11.465	11.465	11.486	11.464	11.512
***b*(Å)**	11.479	11.473	11.486	11.458	11.511
***c*(Å)**	15.598	15.657	15.674	15.704	15.568
***V*(Å^3)**	1777.36	1782.76	1789.27	1784.98	1786.75
Δ*V*/*V* (%)	0	0.30	0.66	0.43	0.53
Energy (eV)	-959.978	-960.029	-960.235	-959.903	-960.084
Δ*E*/*E* (%)	0	0.005	0.027	0.008	0.011

Table. S2. Assignment of Raman spectra of pure KLFC (corresponding to Fig. S5 and S6)

Peak assignment number (Fig. S4)	Raman shifts (cm^{-1})	Band assignments
i	1719	υ(CO)
ii	1647	υ(CO)
iii	1482 (strong)	υ(C=O) stretching
iv	918 (medium)	υ(C-C) stretching
v	858	δ(O-C=O) bending
vi	606	δ(O-C=O) symmetric bending
vii	515	υ(MO ring)

Table S3. Comparison table of polyanionic cathode materials for LIB/NIB application:

Materials	Electrode composition (Material: carbon: binder)	Potential window (V)	Current density (mA g^{-1})	Specific capacity (mAh g^{-1})/ cycle number	Ref.
$KLi_3Fe(C_2O_4)_3$	60:30:10 (Pellet electrode)	1.7-4.3 (NIB) 2.0-4.4 (LIB)	10 10	99/100 86/100	This work
$Na_2Fe(SO_4)_2$	70:20:10	1.7–4.1	0.1C (NIB)	82/50	13
$Na_2Fe(C_2O_4)F_2$	60:30:10	2.0-4.3 (NIB) 2.0-4.4 (LIB)	10 10	~90/50 70/50	17
$Li_3V_2(PO_4)_3$	80:10:10	3.0–4.3	133	~35/1000	12
$Na_2Fe_2(C_2O_4)_3\,2H_2O$	60:30:10	1.7-4.2 (NIB)	10	~90/25	15
$Na_2Fe(C_2O_4)(HPO_4)$	60:30:10	1.7-4.3	10	104/100	18

		(NIB) 2.0-4.5 (LIB)	 10	71/100	
$Li_2Fe(C_2O_4)_2$	60:30:10	1.7-4.3 (LIB)	50	~115/180	16
$NaFePO_4$	80:10:10	1.5-4.0 (NIB)	C/10	~115/200	9
$NaVPO_4F$	80:10:10	2.5-4.3 (NIB)	1C	~58/2500	10
$Na_4Mn_3(PO_4)_2(P_2O_7)$	70:20:10	3.0-4.5 (NIB)	1C	~60/200	11
$Na_6Fe_5(SO_4)_8$/CNTs	80:10:10	2.0-4.5 (NIB)	2C	61.8/1000	S1
$Na_3V_2(PO_4)_2F_3$/SWCNT	70:20:10	2.5-4.35 (NIB)	10C	~85/100	S2
Li_2FeSiO_4	70:20:10	1.5-4.5 (LIB)	C/20	~110/10	S3
CNT@Li_2FeSiO_4@C	70:20:10	1.5-4.5 (LIB)	0.2C	~165/150	S4
$LiFePO_4$	70:20:10	2.0-4.5 (LIB)	0.1 mA /cm^2	~160/20	S5

Triplite $LiFeSO_4F$	80:10:10	2.2-4.6 (LIB)	C/20	~37/80	S6

References

S1 S. Li, X. Song, X. Kuai, W. Zhu, K. Tian, X. Li, M. Chen, S. Chou, J. Zhao and L. Gao, *J. Mater. Chem. A*, 2019, **7**, 14656–14669.

S2 S. Liu, L. Wang, J. Liu, M. Zhou, Q. Nian, Y. Feng, Z. Tao and L. Shao, *J. Mater. Chem. A*, 2019, **7**, 248–256.

S3 X. Lu, H. Wei, H. C. Chiu, R. Gauvin, P. Hovington, A. Guerfi, K. Zaghib and G. P. Demopoulos, *Sci. Rep.*, 2015, **5**, 8599.

S4 T. Peng, W. Guo, Y. Zhang, Y. Wang, K. Zhu, Y. Guo, Y. Wang, Y. Lu and H. Yan, *Nanoscale Res. Lett.*, 2019, **14**, 326.

S5 A. Yamada, S. C. Chung, K. Hinokuma, *J. Electrochem. Soc.*, 2001, 148 (3), A224-A229.

S6 J. Dong, X. Yu, Y. Sun. L. Liu, X. Yang, X. Huang, *J. Power Sources*, 2013, 244, 716-720.

S7 H. Chen, L. L. Wong, S. Adams, *Acta Crystallographica Section B: Structural Science, Crystal Engineering and Materials*, 2019, 75(1), 18–33.

S8 H. Chen, S. Adams, *IUCrJ*, 2017, 4(5), 614–625.

S9 L. L. Wong, K. C. Phuah, R. Dai, H. Chen, W. S. Chew, S. Adams, *Chemistry of Materials* 2021, 33(2), 625-641.